Available online at www.sciencedirect.com

SCIENCE DIRECT®

Earth and Planetary Science Letters 237 (2005) 855–872

EPSL

www.elsevier.com/locate/epsl

An experimental study of the solubility and partitioning of iridium, osmium and gold between olivine and silicate melt

James M. Brenan [a,*], William F. McDonough [b], Richard Ash [b]

[a] *Department of Geology, University of Toronto, Toronto, ON, Canada*
[b] *Department of Geology, University of Maryland, College Park, MD, USA*

Received 14 July 2004; received in revised form 20 June 2005; accepted 22 June 2005
Available online 2 August 2005
Editor: B. Wood

Abstract

We have performed metal solubility and olivine–melt partitioning experiments to understand the behaviour of iridium, osmium and gold during crust–mantle differentiation. All experiments were performed metal-saturated, with molten gold added to suppress nugget formation. Coexisting olivine and iron-bearing basalt glass produced in experiments at 1 bar (10^5 Pa), 1260–1350 °C and fO_2 of FMQ+0.6 to +5.4 were analysed by laser ablation ICPMS. Olivine–melt partition coefficients (Ds) for Ir increase from ~0.4 at FMQ+5.4 to ~2 at FMQ+2.5, with the latter value being consistent with the behaviour of Ir in lavas that have evolved by olivine fractionation. The increase in D_{Ir} with decreasing fO_2 is consistent with an increase in the relative proportion of Ir^{2+} in the melt, as it has an estimated ionic radius close to the "strain-free" value for octahedral coordination in olivine. Gold is highly incompatible in olivine ($D = 1 - 2 \times 10^{-3}$ or less), consistent with its relatively large ionic radius in the Au^{1+} oxidation state. This, together with our previous measurements of olivine–melt partitioning for Pt, Pd, Ru and Rh, indicates that olivine-equilibrated melts will have depletions in Ir, Rh and Ru relative to Pt, Pd and Au, consistent with that measured in primitive, sulfur-poor magmas. Our data provide an upper bound on Os solubility in silicate melt of 10 ppb at FMQ+0.6, even though Os partition coefficients could not be measured. The solubility of Os, Ru and Ir in silicate melt is comparable to the concentrations of these elements in primitive, sulfur-poor magmas, suggesting they could be metal-saturated.

Keywords: platinum group elements; highly siderophile elements; osmium; iridium; gold; partitioning; olivine

1. Introduction

Owing to their refractory nature, and unique geochemical affinity, the highly siderophile elements (HSEs) have found widespread use as tracers of planetary differentiation and evolution. Their behaviour is potentially complex, however, as it is not always clear

* Corresponding author. Tel.: +1 416 978 0281; fax: +1 416 978 3938.
E-mail address: brenan@geology.utoronto.ca (J.M. Brenan).

0012-821X/$ - see front matter © 2005 Elsevier B.V. All rights reserved.
doi:10.1016/j.epsl.2005.06.051

which phases control HSE distribution, with such information often derived empirically (e.g., [1–4]). In mafic and ultramafic igneous systems, olivine is often considered a host for Ir, Os and Ru [1–10]), whereas Pt, Pd, Re and Au are considered to be excluded from the olivine structure [1,3,11]. This behaviour has been confirmed for Ru, Pt, Pd and Re by previous experimental work [12,13]. Conflicting data exist for Os and Ir, however, and it is now demonstrated that these elements do not always behave compatibly during olivine crystallisation [11,14–17]. Further, the abundance of Os, Ir and Au in olivine separates can be extremely low, and highly variable [18–20], suggesting that element "concentrations" may indeed be controlled by variable amounts of inclusion phases (e.g., [21–23]). Accordingly, a detailed understanding of the olivine–melt partitioning of Ir, Os and Au provides the necessary data to evaluate the role of this mineral in controlling the distribution of these elements during melting and solidification.

In the work presented here, we have sought to determine the abundances of Ir, Os and Au in olivine and quenched basaltic melt from high temperature experiments saturated in these metals. Concentration data confirm that Ir is compatible in olivine relative to silicate melt, and that Au is excluded from the olivine structure. The very low abundance of Os in run-product phases precludes an estimate of olivine–melt partitioning, but further affirms the conclusions of Borisov and coworkers [21–23] that other carrier phases, such as Os-bearing alloy, could be important in controlling Os-behaviour in sulfide-undersaturated igneous systems.

2. Experimental techniques

2.1. General

Experiments were performed on samples consisting of a synthetic basalt oxide mixture (corresponding to the Ol+3.1 melt composition of Brenan et al. [12]) plus a premelted bead consisting of gold plus iridium or osmium, held in crucibles fabricated from San Carlos olivine (SCO). To avoid contamination from other noble metals, the basalt composition was not prefused, and melt homogenisation occurred during the initial isothermal soak that preceded the olivine growth step (see below). Both iridium and osmium have much higher melting temperature and low mutual solubility with gold (summarized in [24]), so at run conditions the bead consisted of iridium or osmium crystals surrounded by molten gold. In previous reconnaissance experiments, we found that gold preferentially wets Ir and Os relative to silicate melt, so we employed this technique to prevent the formation of Ir or Os nuggets within the silicate melt, which are a well-known source of analytical difficulty in experiments involving highly siderophile elements [25–28]. Experiments were also doped with a suite of trivalent elements (Sc, and rare earth elements; REEs), so as to assess element partitioning in the context of the Blundy/Wood/Beattie elastic strain model.

2.2. Gas-mixing experiments

All experiments to measure Ir solubility and partitioning were performed using a vertical tube furnace modified for control of fO_2 by gas mixing. Experiment temperatures were monitored using a ceramic-sheathed Pt–Pt10%Rh thermocouple calibrated against the melting point of gold. Control of gas mixtures was achieved using calibrated flow meters; furnace fO_2 was monitored using a Y-doped zirconia oxygen probe (Australian Oxytrol Systems, Ltd.). We did experiments using pure CO_2, and mixtures of Air–N_2, N_2–CO_2 and CO–CO_2, achieving a range in log fO_2 from −1.5 to −4.4, corresponding to ΔFMQ of +5.4 to +1.4 at final run temperatures. Olivine crucibles were suspended in the furnace from the hooked end of a silica rod using a Pd wire hanger; since Pd is largely immiscible with Ir nearly constant activity of these metals is maintained during an experiment, even if the hanger and melt come into contact. Experiments were executed by withdrawing the glass rod to the top of the furnace tube, then sealing the furnace and commencing gas flow. After 20–30 min the sample was lowered manually into the predetermined hot spot, and remained there for the experiment duration. The time–temperature history employed in experiments was designed to promote the growth of large olivine crystals from a melt whose Ir content was homogeneous. To facilitate melt homogeneity, samples were first subject to an isothermal "soak" at 1400 °C, for durations of 48–128 h. After this step, olivine growth was promoted by cooling to 1350 °C at 60°/hr, holding for one hour, then cooling at 1°/hr to 1335 °C.

At the end of the cooling step, experiments were terminated by removing the bottom furnace seal and plunging the sample into cold water.

The above-described experimental technique used starting compositions in which the initial melt contained negligible amounts of Ir. It is possible that some olivine growth could occur during the early part of the isothermal soak step, at a time when the glass composition is still evolving. Therefore, it is important to determine if olivine growth occurs after the melt has reached the concentration now represented by the quenched glass. As a test for this, we also did an experiment in which the melt initially contained ~600 ppb Ir in solution. Given that metal solubilities increase substantially with increasing fO_2, an elevated iridium concentration was accomplished by first subjecting a sample to high fO_2 conditions. Experiment "IrAu rev" was initially soaked at 1400 °C and log fO_2 of −1.5 for 48 h, then the fO_2 was lowered to log fO_2 of −3.1 and the experiment was run with the same time–temperature history as other forward experiments.

2.3. Evacuated silica tube experiments

Owing to the high volatility of Os, experiments involving this element were vacuum-sealed in thick-walled (10 mm OD, 4.1 mm ID) fused silica ampoules along with an oxygen buffer consisting of powdered nickel+nickel oxide (NNO). The olivine crucible was placed on a thin (~1 mm) silica disk immediately above the buffer assemblage. Experiments were done in a bottom-loading box furnace in which the silica tube was placed upright in an alumina crucible on the furnace hearthplate, and temperature was monitored using a calibrated Pt–Pt10%Rh thermocouple located immediately above the sample. Experiments were terminated by lowering the furnace floor, then plunging the sample into cold water. With this method, we did isothermal soak experiments at 1350 °C, and an olivine growth experiment similar to that described above, terminating at 1230 °C, corresponding to log fO_2 values of −6.2 and −7.1, respectively, or FMQ+0.6. A summary of all experiments is provided in Table 1.

3. Analytical techniques

Run products were mounted in 1″ polycarbonate rounds and backfilled with epoxy. After setting, the mount was ground with SiC, and polished with alumina, then colloidal silica. Major element analysis was performed using the Cameca SX50 electron microprobe at the University of Toronto. Conditions used to analyse run-product silicates were 15 kV accelerating voltage and beam currents of 10 nA for glass or 50 nA for olivine. Standards for analysis were natural basalt (Si, Al, Mg, Fe, Ca), albite (Na), bustamite (Mn), and pentlandite (Ni). The metal phase in run products was analysed for Os, Ir, Pd, Fe, Ni and Au using a 20 kV accelerating voltage and 30 nA beam current. Standards for analysis were pure metals (Os, Ir, Pd, Fe, Ni) or Au–Ag alloy (Au). For all

Table 1
Summary of experiments

Expt. ID[a]	PGE added	$T_{superliq}$	$t_{superliq}$ (h)	T_{final}	t_{total} (h)	Log fO_2	ΔFMQ[b]	Other dopants
IrAu-1.5b	Ir	1400	48	1340	65	−1.5	+5.4	Sc, Sm, Tb, Yb
IrAu-2.5	Ir	1399	128	1338	145	−3.1	+3.8	Sc, Sm, Lu
IrAu-3	Ir	1399	96	1338	113	−4.2	+2.7	Sc, Sm, Tb, Yb
IrAu rev[c]	Ir	1408	96	1347	113	−1.5, −3.1	+5.4, +3.8	Sc, Sm, Tb, Yb
IrAu-4.4	Ir	1400	94.5	1343	111.5	−4.4	+2.5	Sc, La
OsAuNNO5	Os	1400	40	1260	65	−7.1	+0.6	Sc, Tb, Yb
OsAuNNO6	Os	1350	112.5	1350	112.5	−6.2	+0.6	None
OsAuNNO7	Os	1350	74	1350	74	−6.2	+0.6	None

[a] All samples contained in San Carlos olivine crucibles. OsAuNNO5, 6 and 7 were run in evacuated silica tubes with Ni+NiO as a buffer, all other samples hung by Pd wire with fO_2 controlled by gas mixing.

[b] log fO_2 with respect to the FMQ buffer, calculated at the final run temperature.

[c] Sample run for 48 h at 1400 °C, log fO_2 = −1.5, then rerun at log fO_2 of −3.1 for the time and temperature specified.

Table 2
Summary of glass and olivine analyses

Expt. ID	Phase	n[a]	SiO_2[b]	Al_2O_3	CaO	MgO	FeO	NiO	MnO	Na_2O	Total	Fe^{3+}/Fe^{2+}, [c]	K_D Fe–Mg[d]
IrAu-1.5b	Glass	15	47.37(0.3)	8.01(0.16)	6.22(0.12)	16.22(0.2)	19.66(0.28)	0.07(0.03)	0.18(0.03)	1.09(0.04)	98.82	0.99	0.29
	Olivine	17	42.45(0.18)	0.08(0.02)	0.12(0.01)	51.18(0.27)	6.01(0.12)	0.44(0.01)	0.11(0.01)	0.02(0.01)	100.4		
IrAu-2.5	Glass	18	47.03(0.26)	7.57(0.11)	6.79(0.1)	16.64(0.17)	20.04(0.24)	0.07(0.02)	0.2(0.04)	0.36(0.03)	98.7	0.56	0.33
	Olivine	15	41.56(0.14)	0.08(0.01)	0.14(0.01)	48.49(0.33)	9(0.25)	0.4(0.03)	0.12(0.02)	NA	99.81		
IrAu-3	Glass	15	52.01(0.23)	9.7(0.1)	8.73(0.12)	15.79(0.17)	13.14(0.28)	0.07(0.03)	0.15(0.03)	0.6(0.04)	100.18	0.24	0.34
	Olivine	16	41.37(0.21)	0.06(0.01)	0.19(0.03)	48.15(0.46)	9.09(0.55)	0.51(0.05)	0.1(0.01)	0.02(0.01)	99.48		
IrAu rev	Glass	17	47.68(0.4)	7.51(0.07)	6.71(0.13)	15.98(0.19)	20.21(0.28)	0.07(0.03)	0.19(0.03)	0.44(0.02)	98.95	0.42	0.31
	Olivine	13	41.1(0.22)	0.07(0.01)	0.14(0.01)	47.17(0.35)	10.09(0.43)	0.42(0.02)	0.13(0.01)	0.02(0.01)	99.13		
IrAu-4.4	Glass	16	52.47(0.32)	10(0.11)	8.79(0.09)	16.24(0.22)	11.78(0.25)	0.06(0.03)	0.15(0.03)	0.49(0.04)	99.98	0.21	0.35
	Olivine	15	41.5(0.47)	0.06(0.03)	0.18(0.01)	48.62(0.68)	8.69(0.37)	0.42(0.02)	0.1(0.01)	NA	99.58		
OsAuNNO5	Glass	15	52.73(0.66)	13.27(0.09)	8.23(0.13)	10.86(0.11)	12.27(0.23)	0.53(0.03)	0.22(0.04)	0.34(0.04)	100.07[e]	0.08	0.30
	Olivine	9	39.90(0.20)	0.08(0.02)	0.12(0.02)	42.09(0.63)	12.20(0.83)	4.51(0.37)	0.17(0.03)	NA	99.13		
OsAuNNO6	Glass	12	51.45(0.50)	10.28(0.13)	9.20(0.27)	16.49(0.18)	12.25(0.33)	0.37(0.04)	0.12(0.04)	0.13(0.04)	100.09		
OsAuNNO7	Glass	12	51.21(0.54)	10.57(0.17)	9.49(0.15)	16.22(0.21)	11.59(0.23)	0.72(0.04)	0.10(0.03)	0.15(0.04)	100.31		

[a] n = number of points analysed.
[b] Number in parentheses is the 1σ error based on n analyses.
[c] Fe^{3+}/Fe^{2+} (molar) in melt calculated for T, fO_2 of experiment using formulation of Kilinic et al. [30].
[d] Molar (Fe/Mg)olivine/(Fe/Mg)melt, equilibrium value is 0.280.32 [31].
[e] Analysis includes 1.60(0.15) wt.% TiO_2.

Table 3
Trace element concentrations (ppm) and olivine/melt partition coefficients

Expt. ID	Log fO_2	T	Au[a]	Phase or ratio	n	Sc[b]	La	Sm	Tb	Yb	Lu	Au	Ir	Os
IrAu-1.5b	−1.5	1340	$Au_{93}Ir_1Pd_6$	Glass	3	74(1)	–	17(0.4)	52(3)	82(2)	–	12.3(0.3)	0.60(0.02)	–
				Olivine	1	9.0	–	<0.02	0.21	1.27	–	<0.01	0.26	–
				Olivine/melt	–	0.12	–	<0.0012	0.0040	0.015	–	<0.0008	0.43	–
IrAu-2.5	−3.1	1338	$Au_{68}Pd_{32}$	Glass	4	94(5)	–	2.2(0.4)	–	–	102(4)	2.7(0.2)	0.079(0.006)	–
				Olivine	4	11.0(0.5)	–	0.0013 (0.0008)	–	–	2.2(0.1)	<0.02	0.049(0.006)	–
				Olivine/melt	–	0.12(0.01)	–	0.00059 (0.00039)	–	–	0.022 (0.001)	<0.0074	0.62(0.09)	–
IrAu-3	−4.2	1338	$Au_{91}Ir_1Pd_8$	Glass	3	107(2)	–	2.2(0.1)	63(5)	119(3)	–	2.13(0.03)	0.0025(0.0005)	–
				Olivine	3	10.5(0.5)	–	0.0039[c]	0.191 (0.003)	1.49(0.07)	–	0.0051 (0.0023)	0.0067(0.0012)	–
				Olivine/melt	–	0.10(0.01)	–	0.00018 (0.00001)	0.0030 (0.0003)	0.013 (0.001)	–	0.0024 (0.0011)	2.7(0.7)	–
IrAu rev	−3.1	1347	$Au_{92}Pd_8$	Glass	3	54(2)	–	4.1(0.1)	51(4)	60(2)	–	3.5(0.1)	0.035(0.009)	–
				Olivine	4	6.7(0.2)	–	0.0015 (0.0004)	0.122 (0.002)	1.04(0.05)	–	0.0025 (0.0006)	0.017(0.001)	–
				Olivine/melt	–	0.12(0.01)	–	0.00035 (0.00010)	0.0024 (0.0002)	0.017 (0.001)	–	0.00071 (0.00017)	0.49(0.13)	–
IrAu-4.4	−4.4	1343	$Au_{90}Pd_{10}$	Glass	4	8(1)	0.36(0.05)	–	–	–	–	2(1)	0.0048(0.0022)	–
				Olivine	4	1.4(0.1)	0.00056	–	–	–	–	<0.004	0.0083(0.0029)	–
				Olivine/melt	–	0.18(0.03)	0.0016 (0.0002)	–	–	–	–	<0.002	1.7(1.0)	–
OsAuNNO5	−7.1	1260	$Au_{95}Ni_5$	Glass	5	160(7)	–	–	179(12)	210(14)	–	0.86(0.16)	–	<0.0048
				Olivine	1	15.4	–	–	0.36	2.33	–	0.17	–	<0.06
				Olivine/melt	–	0.096(0.004)	–	–	0.0020 (0.0001)	0.011 (0.001)	–	<0.20	–	–
OsAuNNO6	−6.2	1350	$Au_{97}Fe_{0.3}Ni_{2.2}$	Glass	5	–	–	–	–	–	–	1.9(0.1)	–	<0.010
OsAuNNO7	−6.2	1350	$Au_{96}Fe_{0.3}Ni_{3.4}$	Glass	5	–	–	–	–	–	–	2.1(0.1)	–	<0.010

[a] Atomic percent in Au melt (other elements < 0.1 at.%).
[b] Number in parentheses is the 1σ error based on n analyses.
[c] Analyses with no standard deviation represent the lowest value of multiple determinations.

analyses, raw count rates were converted to concentrations using a modified ZAF data reduction scheme. A summary of the major element composition of glass and olivine is provided in Table 2. The composition of the Au melt is provided in Table 3, and the results of Ir and Os analysis are discussed below.

Trace elements were determined using the laser ablation ICP-MS facility in the Department of Geology at the University of Maryland. This system employs a frequency quintupled Nd:YAG laser operating at 213 nm, coupled to an Element 2 magnetic sector ICP-MS (ThermoElectron), with He flushing the ablation cell to enhance sensitivity [29]. Conditions for laser ablation analyses (e.g., spot size, beam irradiance, repetition rate) of the phases analyzed in this study were optimized for each sample, depending on element concentration and photon-coupling characteristics. Wherever possible large spot sizes (e.g., ~150 μm) were used for samples having the lowest concentrations of Ir and Os. Factory-supplied time resolved software was utilized for the acquisition of individual analyses. A typical analysis involved ~20 s of background acquisition with the ablation cell being flushed with He, followed by laser ablation for 40–80 s, corresponding to a sampling depth of ~40–80 μm (as measured in sample cross-section). Analyses were collected in a sequence, with the first and last three spectra acquired on standard reference materials (SRM). When possible, 3 to 4 analyses were done on each phase. SRMs employed include NIST 610 and 612 silicate glasses and "in house" standard JB-sulfide, a NiS bead containing 380 ppm Ir and 360 ppm Os. Ablation yields in different phases were corrected by referencing to the known concentration of an element as determined previously by electron microprobe analyses. Ca was used as the reference element for silicate glass and Ni for olivine; this method also provided precise Ni data for the glasses that in turn provided a correction to ablation yields when using the sulfide standard. As a check for interfering isobars, element concentrations were determined using multiple isotopes, when possible. The following isotopes were used to determine element concentrations reported in this study: ^{45}Sc, ^{159}Tb, ^{173}Yb, ^{175}Lu, ^{189}Os, ^{193}Ir, ^{197}Au.

We also did a series of calibration analyses for Ir and Os on a variety of silicate glasses, olivines, sulfides, kamacites and taenites to evaluate the precision and accuracy of the method used in this study. Meteoritic samples, include co-existing kamacite, taenite, and troilites from Canyon Diablo, taenite from Nedagolla and Hoba, coexisting kamacite, taenite and olivines from Milton and Eagle station and kamacite from Coahuila, were analyzed. Other materials include steels NBS 809b and NIST 1158. These analytical experiments provide data on background, isobaric interferences and detection limits and also demonstrated a lack of matrix dependency at the level of precision of these analyses ($\pm 1\sigma$ at circa 5% to 25%). The limits of detection for Os and Ir in olivine and glass depend on the specific conditions of analysis, and when optimised, can be as low as 100 ppt (3σ above background). A summary of the trace element content of glass and olivine and calculated olivine/melt partition coefficients is provided in Table 3.

4. Results and discussion

4.1. Textural observations

The textural development of run-product phases from an experiment done in the gas-mixing furnace is portrayed in Fig. 1. Olivines produced in such experiments are relatively large (100+μm), in some cases "lantern" shaped, and generally euhedral, with occasional glass inclusions. Olivine crystals extend from the walls of the crucible, separated by a narrow septum, or occur as isolated phenocrysts. Olivines produced in the evacuated silica tube experiment are somewhat smaller (25–60 μm), although the overall morphology is similar. All experiments reported in this paper remained saturated in Ir+Au or Os+Au as evidenced by the presence of these phases in sectioned run-products. Iridium and osmium occur as subhedral crystals completely immersed in a globule of quenched gold melt. Ir crystals are typically 10–50 μm in diameter, whereas Os crystals are in the 1–5 μm size range.

4.2. Alloy compositions

Electron microprobe analyses of Ir crystals in run products show less than 0.1 wt.% Au, Fe, Ni or Pd, indicating that the activity of Ir in our experiments was unity. Os crystals were much more difficult to analyse, owing to their very small size, and conse-

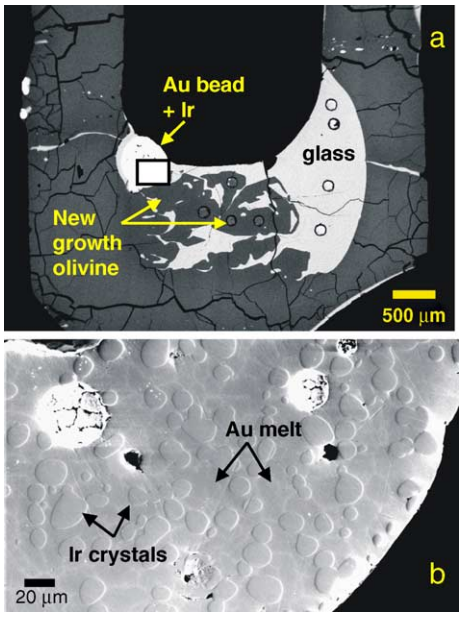

Fig. 1. a) Backscattered electron image of the sectioned olivine crucible from experiment IrAu-2.5 showing the quenched Fe-bearing silicate melt (=glass) and olivine phenocrysts (=new growth olivine). Circular features correspond to areas ablated for ICP-MS analysis. b) Secondary electron image showing a closeup of the white rectangular region in a) containing the Ir–Au bead. High relief, subhedral iridium crystals are immersed in quenched gold melt. No iridium crystals were found isolated from the Au bead, indicating preferential wetting of the iridium by the gold relative to the silicate melt.

quently all analyses contain some Au, which presumably is derived from X-rays generated in the surrounding melt. The "cleanest" Os analyses yielded ~5 wt.% Au, so we assume that the activity of Os in our experiments is also near unity. The quenched Au melt contained minor abundances of Os, Ir, Fe and Ni (1 wt.% or less), but variable, and somewhat elevated abundances of Pd (to a maximum of 20 wt.% in experiment IrAu-2.5a; Table 3) in samples run in the gas-mixing furnace. In those experiments, the sample was hung by a Pd wire attached to the olivine crucible, so some Pd diffused into the crucible through the thin selvage of melt present on the crucible surface, or lining throughgoing cracks in the crucible wall.

4.3. Major element equilibrium

Electron microprobe analyses across individual olivines reveal them to be homogeneous, as the standard deviation in analyses are generally similar to errors from counting statistics. Glass analyses from analytical traverses both across and down the length of a run-product reveal the same level homogeneity. Such results are also confirmed by the reproducibility of the minor element (Ca, Mn and Ni) content of crystals and glasses measured by LA–ICP-MS. In addition to phase homogeneity, phenocryst–melt equilibrium appears to be achieved, as judged by major and minor element partitioning systematics. Using the formulation of Kilinc et al., [30], we calculated the FeO and Fe_2O_3 abundances in run-product glasses from the total FeO measured by electron microprobe. The olivine–melt FeO–MgO exchange coefficient was then calculated for coexisting phenocryst–glass pairs (Table 2), and all values are close to the canonical value of 0.30 ± 0.02 determined by Roeder and Emslie [31]. Olivine–melt partition coefficients for calcium are also in agreement with the equilibrium value of 0.021 determined by Jurewicz and Watson [32].

4.4. Trace element behaviour

4.4.1. Phase homogeneity

Examples of time-resolved ICP-MS spectra for glass and olivine are provided in Fig. 2. In general, both phases show a homogeneous distribution of Sc, Tb, Yb and Lu, as judged by the uniform count rates for these elements with ablation time (=depth into sample). The light rare-earth elements La and Sm are highly incompatible in olivine, and as a result are good tracers of melt contamination in the olivine analyses. Au concentrations in run-product glasses are uniform, whereas Au abundances in olivines are very low (Fig. 2a), but in some cases show variation which correlates with La or Sm. We attribute this heterogeneity to the presence of a small amount of melt contamination in the ablated area and reported concentrations are determined for only those olivine domains having the lowest La or Sm contents. Partition coefficients for La and Sm are based on the lowest concentration measured in olivine crystals from a specific experiment. Phase homogeneity for Ir was encountered over the range of fO_2 investigated (Fig. 2b,c), despite decreases in metal content arising from reduced solubility at lower fO_2. Occasional Ir alloy inclusions were encountered, but they occurred as short duration, high intensity

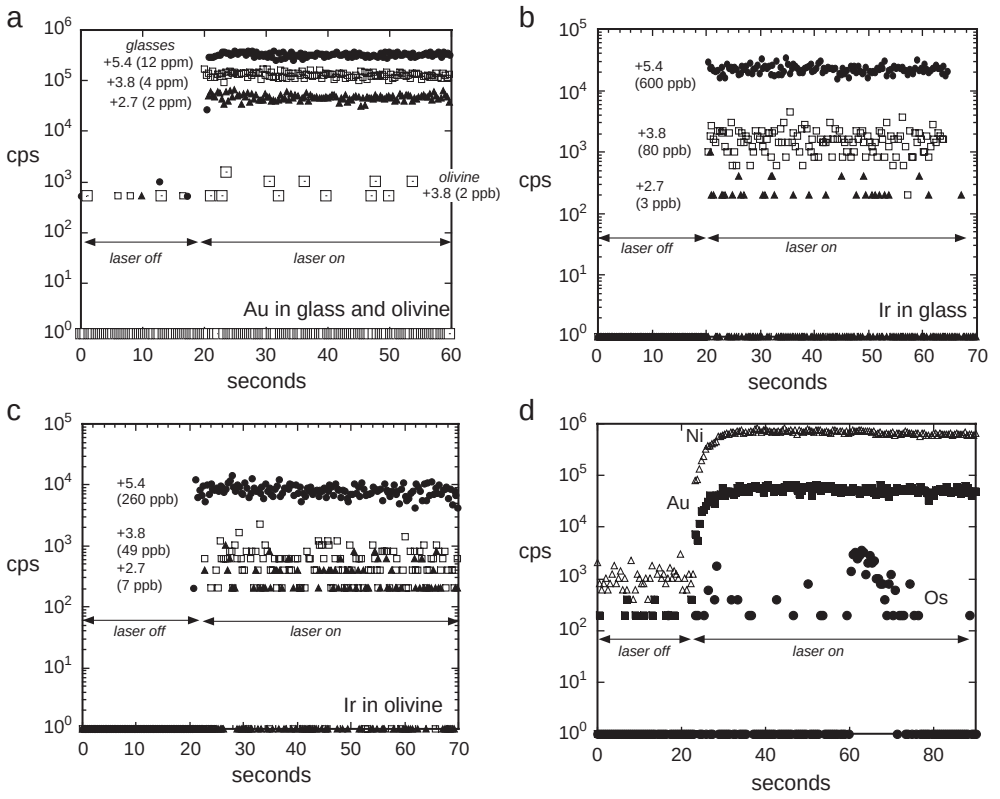

Fig. 2. Examples of time-resolved spectra from LA–ICP-MS analysis of glasses and olivines produced in this study. a) Au in glass and olivine, b) Ir in glass, c) Ir in olivine and d) Ni, Au and Os in glass from experiment AuOsNNO6. The Os spectrum in d) illustrates the type of count rate heterogeneity (particularly at 60–80 s) which we attribute to undissolved metal particles. Particle-free Os-saturated glasses (not shown) yielded count rates indistinguishable from background. In each case, instrument background is collected for ~20 s, followed by laser ablation of the sample for ~80 s. Data are labeled in terms of relative log fO_2 (ΔFMQ), and the calculated metal concentration. For the purposes of plotting, count rates corresponding to zero are plotted as one. A count rate of 203 cps corresponds to the accumulation of one count during a 5 ms dwell on a given mass, hence the lack of data between 1 and 203 cps.

aberrations in an otherwise uniform time-resolved profile. Such features were easily avoided during the data reduction procedure.

The silicate phases produced in Os-saturated experiments yielded count rates for Os that were usually at background values, corresponding to Os concentrations in glass at or below 10 ppb and in olivine below 60 ppb. As was the case for iridium, the time-resolved spectra for Os-saturated glass samples was sometimes punctuated by discrete Os-rich domains (Fig. 2d), but other areas of the same sample were free of heterogeneities; minimum concentrations reported in Table 3 are for only those portions of the glass spectra with low and uniform count-rates. The presence of Os-rich domains is similar to that reported previously by Brenan et al. [12] for Os-saturated glasses from gold-free experiments, although the glasses from the present study contain far fewer Os "spikes". Signal heterogeneity was also reported by Ertel et al. [25,26] for Rh, Pt and Re-saturated glasses equilibrated at low fO_2, and this behaviour was interpreted to be due to the ablation of undissolved metal micronuggets during sample analysis. Lindstrom and Jones [28] also attributed the Ir heterogeneity in bulk experimental run-products analysed by INAA as arising from small amounts of dispersed metal. Inasmuch as the Os content of run-product glasses or olivine are undetectable, olivine–melt partition coefficients for this element cannot be determined. However, as discussed below, the low Os solubilities implied by our

data have implications for possible Os hosts in natural magmatic systems.

4.4.2. Trace element equilibrium

The generally homogeneous distribution of Sc, REEs, Au and Ir within run product phases is an important observation in support of phase equilibrium. However, a concern arises because some studies have shown that metal-silicate melt equilibrium can be sluggish (e.g., [25–27]), therefore it is important to determine whether the metal content of the melt has reached an equilibrium value such that olivines sample a uniform reservoir during growth. The lack of metal zonation in olivines certainly suggests that melt metal contents were probably uniform during growth, and we have also successfully reproduced partition coefficients for Ir by synthesis paths involving large changes in melt metal content. Experiment "IrAu rev" involved subjecting the melt to high fO_2, hence dissolving high Ir concentrations (~600 ppb based on the results of IrAu-1.5b), then low fO_2, in which the melt metal content decreased to 35 ppb. The two-stage experiment yielded similar melt metal contents and identical partition coefficients as the forward experiment done at lower fO_2 (IrAu-2.5a; Table 3). This result is also consistent with the findings of Brenan et al. [12], who showed that Ru and Pd partitioning could also be reproduced following changes in fO_2 in experiments of similar duration. In addition to reproducibility by different synthesis paths, Brenan et al. [12] found that partition coefficients for Rh and Pd are the same for experiments in which the melt homogenisation step lasted from 24–135 h, which overlaps with the homogenisation timescale of our experiments.

4.4.3. Comparison with previous metal solubility determinations

Comparison of Ir, Au and Os solubilities measured in our experiments with those determined previously are provided in Fig. 3. With the exception of the work on Ir solubility by Amosse et al. [33], which employed an Fe-bearing basalt analogue, all previous solubility determinations for these elements used an Fe-free diopside–anorthite eutectic composition. Our iridium solubilities are in good agreement with values measured by Borisov and Palme [34] involving experiments done at 1300 and 1480 °C (Fig. 3a), although our results extrapolate to lower solubility with decreasing fO_2 (see discussion of this below). Ir solubilities reported by O'Neill et al. [27] for experiments done at 1400 °C are ~10× higher than those measured in this study, or by Borisov and Palme [34], although the solubility–fO_2 trend is generally similar. The origin of this difference is unclear, although O'Neill et al. [27] used a stirred crucible technique, whereas our experiments, and those of Borisov and Palme [34], were static. Perhaps the stirred crucible technique maintains small particles in suspension, which are subsequently included in the bulk analysis. Results reported by Amosse et al. [33] for experiments run at 1430 °C show that Ir solubility *increases* with decreasing fO_2. Their explanation for this apparently anomalous behaviour is that Ir dissolves as a neutral complex in silicate melt, and that this dissolved species reacts with oxygen to produce an oxide film on the Ir metal surface (so-called passivation). This model predicts that the Ir solubility should increase with decreasing fO_2, then level off at a value of ~10 ppm at log fO_2 of −8 and below [35]. Despite the possibility of trapped Ir particles sampled during bulk analysis, neither Borisov and Palme [34] nor O'Neill et al. [27] measured Ir solubilities that approach such high values in that fO_2 range. The reduction in solubility with decreasing fO_2 measured in this and previous studies imply that Ir is reacting with oxygen to dissolve as a metal oxide species (cf., O'Neill et al. [27]). This type of solution behaviour has now been documented for most of the highly siderophile elements [21,25–27,36–38] in Fe-free systems, and some results have been confirmed for Fe-bearing compositions (this study; [12]). The results of Amosse et al. [33] imply a completely different solution mechanism, and given the general similarities amongst previous studies in experiment design and execution, the origin of this discrepancy is unclear.

Our Au solubility data show good agreement with values determined by Borisov and Palme [38], although in detail, some of our values appear to be lower than their solubility–fO_2 trend. This could reflect that the molten Au in our experiments contains some Pd (3–38 at.%), and we have not corrected our solubilities to unit activity.

The Os solubilities of≤10 ppb we have measured for melts coexisting with Os alloy are close to values reported by Borisov and Walker [23] for experiments

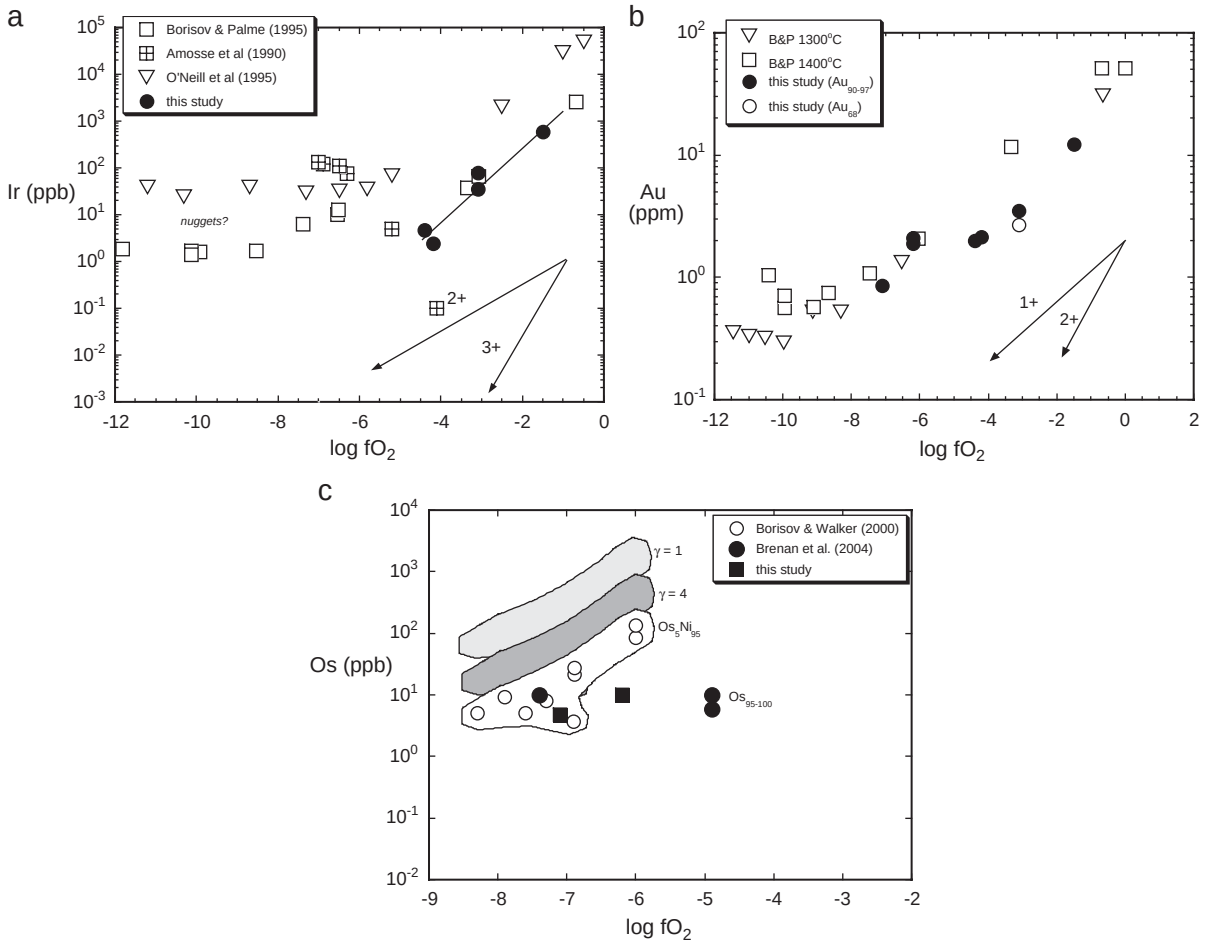

Fig. 3. Comparison of iridium (a), gold (b) and osmium (c) solubilities in silicate melts determined in this study with values measured previously. In a) and b) the vectors labeled 1^+, 2^+ and 3^+ correspond to the variation in solubility with fO_2 expected for metals dissolving in the silicate melt as 1^+, 2^+ and 3^+ cations. The solid curve through the iridium solubility data from this study is a best fit line. In c), the open circles correspond to the osmium content of glasses coexisting with Os_5Ni_{95} (atomic basis) alloy. Filled areas show how glass concentrations would shift if the metal phase were pure Os, assuming γ_{Os} in the alloy = 1 and 4, the latter by analogy to the Re–Ni system (after [28]). Data from this study and Brenan et al. [12] are maximum values, as Os contents were either low, but heterogeneous or undetectable.

done over a similar range in fO_2, at 1400 °C in which samples were analysed by bulk techniques (Fig. 3c). However, the latter results were obtained for melt coexisting with Os_5Ni_{95} alloy, so activity-corrected glass concentrations will be 4–18 times higher (depending on the solution model; Fig. 3c) for pure Os. Relatively speaking, our maximum solubilities for glass coexisting with $Os_{>95}$ are lower than the saturation values derived from the Borisov and Walker [23] experiments. Although Os can be somewhat volatile at the fO_2 at which we did our experiments, sealing the samples in fused silica ampoules has eliminated volatility as a possible cause of the low solubilities we have measured. This difference in Os solubility may be a melt composition effect, or could possibly be an analytical artifact. The diopside–anorthite eutectic melt used by Borisov and Walker contains similar Si, Al and Mg, but much lower Fe, and higher amounts of both Ca and Ni compared to the compositions produced in our study. It is conceivable that the activity coefficient for Os is lower in the melt used by Borisov and Walker [23] as a consequence of these

compositional differences. Indeed, previous work has shown that changes in melt composition may affect the solubility of Pt [39] and Pd [40]. It is also possible that the high values measured by Borisov and Walker [23] are a consequence of glass contamination by Os-rich inclusions. As described above, Os-saturated glasses produced in this study contain Os-rich domains, as observed during time-resolved analysis (e.g., Figs. 2d and 3d of [12]). Inclusion of such material in a bulk analysis obscure the low Os concentrations intrinsic to the glass, and overestimate the Os solubility in such experiments. In conclusion, we suggest that the maximum Os solubility measured in our study is probably a better representation of Os saturation levels in natural sulfur-free mafic melts, given the close correspondence of our melts to natural compositions. Further, we believe we have managed to minimise the contribution of Os-rich material in estimating solubilities.

4.4.4. Estimation of Ir and Au valence state from solubility data

The above-described solubility–fO_2 relations can be used to estimate the valence state of Ir and Au in molten silicate, which is useful for understanding olivine–melt partitioning of these elements, as will be discussed in Section 4.4.6. The reaction describing the solution of metal (M) into silicate melt takes the form:

$$M_{\text{metal}} + x/4O_2 = MO_{x/2,\text{melt}}. \quad (1)$$

where $MO_{x/2}$ represents the metal oxide species dissolved in the silicate melt, and x is the valence state of M in solution. The equilibrium constant for this reaction is:

$$K_{\text{eq}} = \frac{\left[MO_{x/2}^{\text{melt}}\right]}{\left[M^{\text{metal}}\right] fO_2^{x/4}} \quad (2)$$

in which square brackets denote activity. For the pure metal, $[M^{\text{metal}}]=1$, and the activity of metal in the melt can be related to its mole fraction (X) through the activity coefficient (γ). Taking the log of both sides yields the expression:

$$\log K_{\text{eq}} = \log\gamma_M^{\text{melt}} + \log X_M^{\text{melt}} - \frac{x}{4}\log fO_2. \quad (3)$$

Assuming that the activity coefficient for metal in the melt is a constant, then this value, $\log K_{\text{eq}}$ and the conversion between mole fraction and concentration by weight (C) can be combined into a single constant, to yield:

$$\frac{x}{4}\log fO_2 = \text{constant} + \log C_M^{\text{melt}}. \quad (4)$$

Thus the slope of a plot depicting $\log C$ as a function of fO_2 can be used to extract the valence state. The Ir solubility data of O'Neill et al. [27] yielded a slope of 0.5 in the oxidizing region (log fO_2 of -0.5 to -5) suggesting solution as Ir^{2+}. Data from Borisov and Palme [34] yielded variable slopes, suggest the predominance of Ir^{3+} from log fO_2 of -0.7 to -4, then Ir^{1+} from log fO_2 of -4 to -10. O'Neill et al. [27] interpreted the lessening of slope in the solubility vs. fO_2 trend (Fig. 3a) at log $fO_2 < -4$ as a result of sampling suspended microparticles during bulk analysis. This effect has been evoked to explain similar behaviour for Pt and Rh solubility [25], in which melt heterogeneity was documented. Therefore, we view the Ir^{1+} valence inferred by Borisov and Palme [34] as possibly an artifact of inclusion sampling at low fO_2. The slope obtained in this study (0.8) is similar to that determined by Borisov and Palme in the oxidising region, and is consistent with a mixed valence of at least 3^+ and lower. Borisov and Palme [38] calculated a slope of 0.25 from the Au solubility–fO_2 relation they obtained, consistent with Au dissolving as a $1+$species in the silicate melt. The Au solubilities we measured are in accord with that result.

4.4.5. Olivine–melt partition coefficients

At log fO_2 of -1.5 and -3.1, the partition coefficient for Ir is ~0.6, whereas the value increases to ~2 at log fO_2 of -4 or less. This behaviour contrasts with Sc, Tb and Yb, whose partition coefficients remain constant with decreasing fO_2 (Fig. 4a). Variation in D_{Ir} with fO_2 parallels that determined previously for Rh and Ru [12], and indeed, partition coefficients for Ir, Ru and Rh converge to similar values at the lowest fO_2 investigated. Partition coefficients for Au are uniformly low ($1-2\times10^{-3}$ or less), with no apparent change with fO_2, although any relation is probably obscured by the relatively low precision of these measurements. The incompatibility of Au in olivine that we have documented is consistent with the results

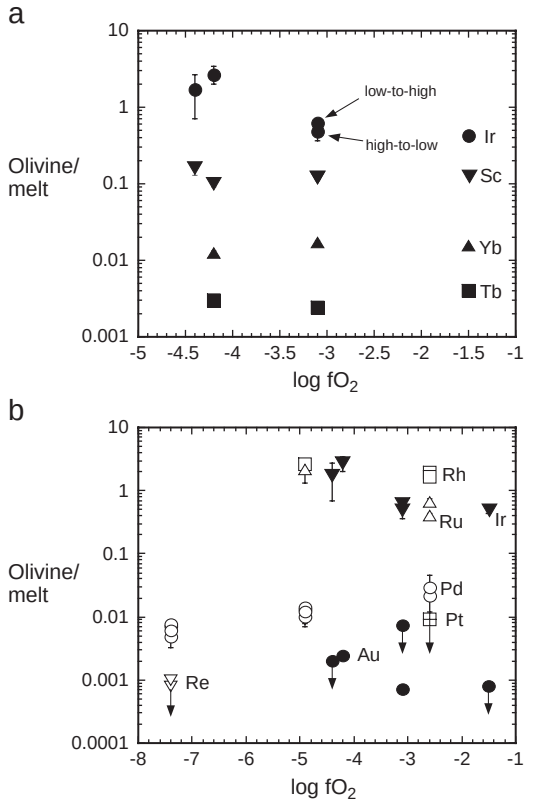

Fig. 4. a) Olivine–melt partition coefficients for Ir, Sc, Yb and Tb as a function of log fO_2. Note the constant values obtained for Sc, Yb and Tb, whereas the partition coefficient for iridium increases with decreasing fO_2. Data points labeled as "high-to-low" and "low-to-high" are for experiments "IrAu rev", and IrAu-2.5, respectively, and refers to the change in Ir content of the melt prior to olivine growth. b) Summary of olivine melt partition coefficients for Re, Au and the platinum group elements (this study and [12]) as a function of log fO_2. Data with downward-pointing arrows are maximum values, as concentrations of the elements of interest in run-product olivine are undetectable.

of Righter et al. [13], who measured an olivine–melt D for Au of 0.12 at log fO_2 of −1.65 and 1300 °C. Our previous work [12] and that of Righter et al. [13] has shown that Pt, Pd and Re are moderately to strongly incompatible in olivine (Fig. 4b), indicating that olivine can fractionate the highly siderophile elements during melting and solidification.

In general, the partition coefficients we have measured are in reasonable agreement with values inferred from natural samples. For example, based on correlations between HSE abundance and MgO content of komatiites, Brugmann et al. [1] estimated a value for D_{Ir} of 1.8 and D_{Au} of less than one. Somewhat lower values for D_{Ir} of 0.8 and 0.35–0.5 in suites of primitive, high MgO magmas, have been reported [3,4]. It is important to note, however, that the accuracy of partition coefficients for HSEs estimated from natural samples can be compromised if discrete carrier phases, such as Os–Ru–Ir alloy also co-precipitate during olivine crystallization (as discussed below). Thus, the reduction in Ir with decreasing MgO observed in the Brugmann et al. study could be a result of this effect. Also, the intrinsic Ir content of olivine and "liquid" compositions determined by Puchtel and coworkers may be overestimated (to a degree which is unknown), if analysed samples contain included alloys.

4.4.6. Interpretation of the iridium and gold partitioning data

It is now well-established that mineral–melt partitioning of trace elements can be accurately modeled with knowledge of elastic moduli for the host mineral, the charge and ionic radius of the substituent ions, along with partitioning data for the major element these ions replace [41,42]. The basis for such models is that the energetics of partitioning is dominated by the amount of elastic strain associated with placing a cation on a particular crystallographic site when the radius of the cation differs from the optimal or "strain-free" radius for that site. Beattie [41] and Purton et al. [43] demonstrated that olivine–melt partition coefficients for elements in VI-fold coordination adhere well to the elastic strain model, with values decreasing in proportion to their mismatch from the optimal radius for the octahedral site (r_o). In previous work [12], we have shown that this model provides a reasonable framework for understanding the olivine–melt partitioning of Re, Ru, Rh, and Pd, although D_{Pt} was much lower than predicted based on a 2+cation charge. Despite this previous success, it is important to note that the elastic strain model is unlikely to provide a complete description of the olivine–melt partitioning of HSEs, simply because the model implicitly assumes that bond formation involving substituent elements and oxygen is wholly ionic. This is not the case for the HSEs in general, given the differences in electronegativity between these elements and oxygen is relatively small (~1), implying bonds that are only 20–30% ionic [44]. In light of the predominantly

covalent character of HSE–oxygen bonding, and the involvement of d-shell electrons, it is also likely that the energetics of partitioning could be influenced by crystal field effects. For Au^{1+}, which has a d^{10} outer shell configuration, this effect may be minimal, whereas it is possible that Ir^{2+}, with a d^7 outer shell configuration, may achieve some measure of stability (akin to Co^{2+}) in octahedral coordination. Given a partial ionic character of the HSE–oxygen bond, the elastic strain model may provide a framework to interpret the change in iridium partitioning with fO_2 and the large fractionation of Ir from Au.

Accordingly, we use the Blundy–Wood version of the elastic strain model, where the relation between the partition coefficient, D_i, for a particular cation of radius r_i, is expressed as:

$$D_i = D_o \exp\Big(-4\pi E N_a \Big(r_o/2(r_o - r_i)^2 - 1/3(r_o - r_i)^3 \Big)/RT \Big) \quad (5)$$

in which D_o is the value of the partition coefficient corresponding to the optimal radius for substitution into the olivine octahedral site, r_o and E is the Young's modulus for the site. The optimal radius for the olivine octahedral site, as calculated by Beattie [41] is 0.058 nm using the volume between "just touching" spherical oxygen atoms at the edges of an octahedron, and is the value adopted here (cf. the value of 0.063 nm used by Purton et al. [43]). The oxidation state of the HSEs in silicate melts can be subject to some uncertainty, given that such information is typically derived from the variation in metal solubility with fO_2 (as described above). Not only is the interpretation of the solubility–fO_2 relation highly dependent on the quality of the solubility data, but the metals could be dissolved in multiple valence states, which may change with fO_2. Based on the previous discussion, we have assumed Ir^{2+} and Ir^{3+} as possible oxidation states over the fO_2 range of our experiments. The ionic radius of Ir^{3+} in VI-fold coordination is taken from Shannon and Prewitt [45,46], and that for Ir^{2+} is estimated by extrapolating the Shannon and Prewitt [45,46] data assuming a linear relation between ionic radius and charge. The data obtained in our study are sufficient to determine D_o and E for 2^+ and 3^+ cations by regressing a linearized form of Eq. (5) (note that data for La and Sm partitioning are not used in these calculations, as we consider these to be maximum quantities). These values can in turn be used in combination with Eq. (5) to calculate partitioning parabola for our experiments. In Fig. 5 we compare the partition coefficient for Ir corresponding to the ionic radius of both Ir^{2+} and Ir^{3+} with the predicted 2^+ and 3^+ partitioning relations. At log fO_2 of -1.5 and -3.1, both D_{Ir3+} and D_{Ir2+} fall between the predicted values, whereas at log fO_2 of -4.2, D_{Ir2+} is an excellent match with that calculated for a 2+cation having the same ionic radius. In the context of this model, the relatively large value of D_{Ir} is a consequence of Ir^{2+} having an ionic radius close to r_o, which is the "strain-free" value for octahedral coordination. This result implies that Ir becomes more compatible in olivine with decreasing fO_2 because of an increased proportion of Ir^{2+} in the melt. Our partitioning data therefore suggests that Ir exists in mixed 2+ and 3+ valence states at high fO_2. The high fO_2 solubility data from Borisov and Palme [34], and that obtained in this work, permit valence states of 3^+ and lower, consistent with the Ir partitioning systematics.

As outlined previously, Au solubility systematics indicate the predominance of Au^{1+} in molten silicate, which in VI-fold coordination has an ionic radius of 0.15 nm. The relation between D_o and ionic charge proposed by Wood and Blundy [47], combined with values of D_o for 2+ and 3+ cations measured in this study, results in a D_o for 1+ cations of ~0.25. An estimate of E for 1+ cations in olivine can be derived using Eq. (5) combined with previously published data for olivine–melt partitioning [48], yielding a value of ~110 GPa. The partition coefficient predicted for Au^{1+} is $\sim 10^{-15}$, which is a consequence of the very large ionic radius of Au in this low oxidation state. The partition coefficients we measured are $1-2\times10^{-3}$ and less, so some values are not inconsistent with the very low D predicted for Au^{1+}. It is possible that the absolute partition coefficients of $1-2\times10^{-3}$ we have measured reflect either some contribution from melt to the olivine Au signal or the presence of Au with a higher oxidation state in our experimental system. As an example of the latter, the ionic radius of Au^{3+} in VI-fold coordination is 0.99 nm [45,46], and the predicted partition coefficient is $\sim 5\times10^{-4}$, which is more similar to the values we have measured. In either case, the Blundy–Wood model accounts for the low partition coefficient for Au as being due to the large difference in the size of

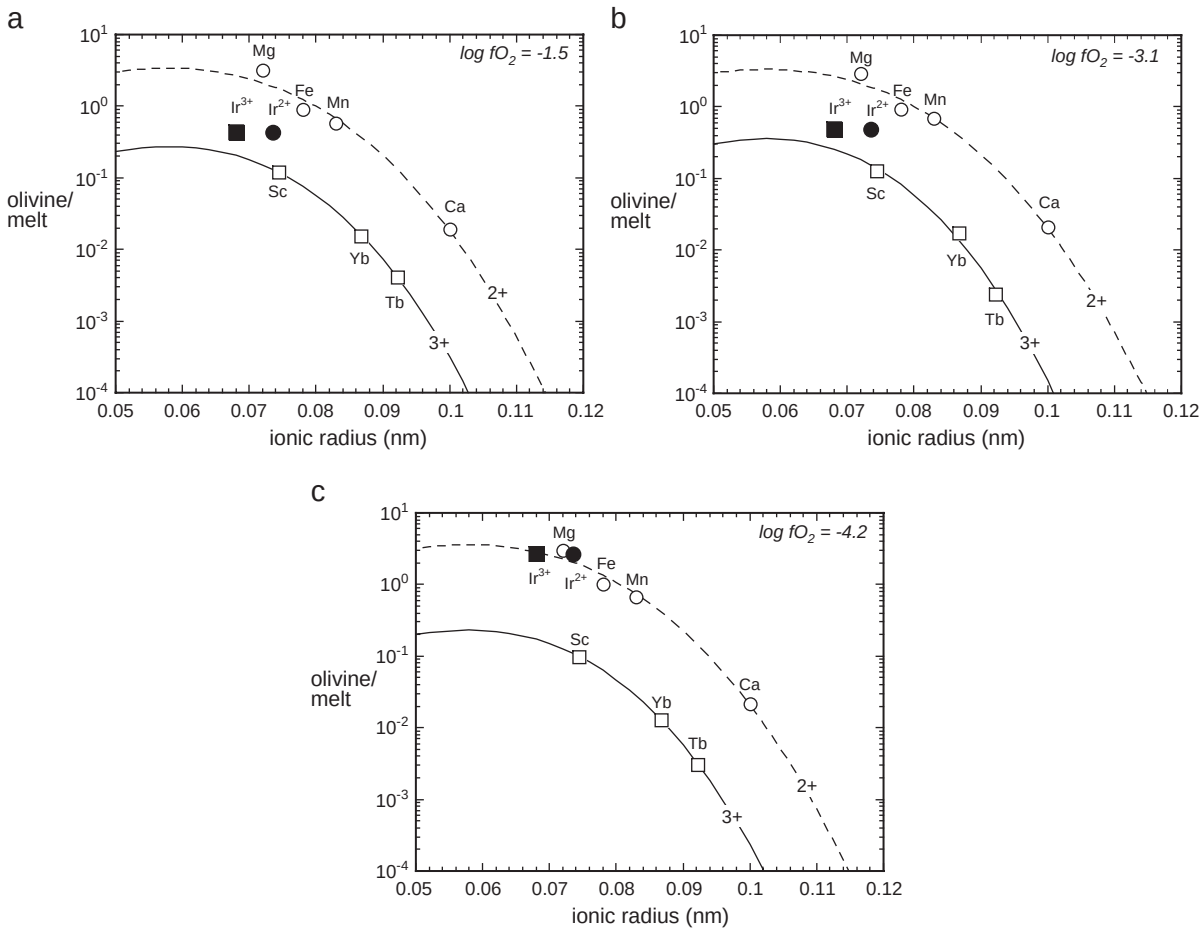

Fig. 5. Comparison of olivine/melt partition coefficients predicted using the lattice–strain model of Blundy and Wood [30] and those measured in this study at log fO_2 of a) −1.5 (IrAu-1.5b), b) −3.1 (IrAurev) and c) −4.2 (IrAu-3). Ionic radii are for VI-fold coordination and the cation charge indicated. The D for Fe^{2+} is calculated using the melt Fe^{3+}/Fe^{2+} ratio from Table 2, and assuming olivine contains only Fe^{2+}. Note the near-coincidence of the Ir^{2+} partition coefficient at low fO_2 with the curve defined for 2^+ cations.

the Au cation relative to the optimal value for octahedral coordination.

4.4.7. Implications of the osmium solubility data

Minerals rich Os, Ir, and Ru, including laurite (RuS_2), and alloys such as rutheniridosmine (nomenclature of [49]), have been repeatedly observed as inclusions in chromian spinel and ferromagnesian silicates crystallized in rocks derived from mafic and ultramafic magmas. The list of occurrences of laurite and Os–Ir–Ru–rich alloys with this paragenesis is extensive (e.g., ophiolites [50–53]; layered intrusions [54–56]), with these phases nearly always being the most abundant platinum-group minerals (PGM) present. The common euhedral shape of Os–Ir–Ru mineral inclusions, coupled with the occurrence of chromian spinel, olivine and pyroxene included within alloy grains (Heazlewood River Complex [57]), suggests co-precipitation at magmatic conditions. Such observations offer strong textural evidence that laurite and/or alloy may be an early crystallizing host for the PGEs during solidification of mafic and/or ultramafic magmas [6,57].

Borisov and Palme [22] provided a comprehensive summary of existing HSE solubility data, including an assessment of the effects of T, fO_2 and melt FeO content. They showed that mantle-derived magmas crystallizing at or below the FMQ buffer have HSE

contents sufficient to be saturated in Ru+Ir-bearing alloy. Data from our study provides an estimate of the maximum Os concentrations in basaltic melts required for saturation in osmium metal. The lowest solubility we have measured (<10 ppb) corresponds to that portion of a glass for which no heterogeneity in Os content was encountered, and so we consider this value as being closest to the intrinsic glass concentration limit. This maximum solubility is comparable to those estimated for Ru and Ir at the same oxygen fugacity [22], and given that there is extensive solid solution in the Ru–Os–Ir system [24], it is plausible that these elements will saturate as a multicomponent alloy in natural magmas. However, owing to a very limited database, there is still some uncertainty as to how factors other than fO_2, such as fS_2, temperature and melt composition, influence Os, Ir and Ru solubility, so the inferences based on the existing experimental solubility data should be viewed with caution.

The removal of an alloy containing Os, Ir and Ru in a carrier phase like olivine could account for the reduction of those elements with decreasing MgO, as is typically observed in high MgO lava suites [1–4]. Many high MgO suites are also saturated in chromite, which cannot only dissolve high concentrations of Ru and Ir [13], but may also serve as a site of metal saturation induced by local fO_2 reduction by the preferential uptake of Fe^{3+} and Cr^{3+} into the chromite structure [58,59]. If a magma is already close to saturation, local reduction followed by metal entrapment by chromite growth may also serve to remove Ru, Os and Ir during differentiation. In terms of other HSEs, Borisov and Palme [22] concluded that although the solubilities of Au and Pd are too high for metal saturation in primitive magmas, saturation in Pt–Fe alloy is likely. The behaviour of Pt, Pd and Au in sulfide-undersaturated primitive magmas is similar, however, and all three elements increase in abundance during progressive crystallization, as gauged by decreasing melt MgO content [1–4]. Thus, these elements are incompatible in the crystallizing phase assemblage. Clearly, the progressive increase in Pt abundance during differentiation is inconsistent with metal saturation and removal. Borisov and Palme [22] have suggested that Pt metal formation in primitive magmas may be inhibited by high fO_2 in their source regions, but the required value of FMQ+2 is at the upper end of estimates for the source of komatiites [60] and most terrestrial magmas [61]. Besides increased fO_2, other factors that have been shown to enhance Pt solubility are melt depolymerization [39] and increased fS_2 [62]. The melt composition used in the Pt solubility experiments on which the Borisov and Palme conclusion is based [21] corresponds to the diopside–anorthite eutectic, which has a non-bridging oxygen/tetrahedrally coordinated cation ratio (NBO/T) of ~1. For primitive, high MgO lavas of komatiite composition, NBO/T is ~2, indicating such melts are significantly less polymerized than those used in the experiments. Although the sulfur fugacity at which komatiites erupt is unknown, such magmas are clearly sulfur-bearing, as base metal sulfides are a common late-stage phase. Thus, it is possible that these factors may serve to enhance Pt solubility sufficiently to inhibit saturation.

5. Summary and conclusions

The results of our olivine–melt partitioning experiments for iridium show an overall increase in partition coefficient with decreasing oxygen fugacity, and that Ir becomes compatible in olivine at log fO_2 of −4.1. This increase in D_{Ir} is consistent with higher levels of Ir^{2+} with decreasing fO_2, as Ir in the 2+ oxidation state is close in size to the "strain-free" radius for partitioning onto the octahedral site in olivine. The incompatibility of Au in the olivine structure is consistent with the elastic strain model given the large ionic radius of Au^{1+}, relative to the optimal strain-free radius. Combining this with our previous results for Pt, Pd, Ru and Rh indicates that olivine-equilibrated melts will have depletions in Ir, Rh and Ru relative to Pt, Pd and Au. Such behaviour is similar to that found for primitive, high MgO magmas, which typically have Ir and Ru abundance levels slightly less than values estimated for primitive mantle, with Pt, Pd and Au being at or above primitive mantle levels (e.g., [1–4]). We have also found that the solubility of Os in silicate melt is very low, similar to that for Ru and Ir, and close to the concentrations of these elements in primitive, sulfur-poor lavas. The removal of an Os–Ru–Ir–bearing alloy included in a mineral carrier phase like olivine or chromite is a means of explaining the depletions of these elements in more evolved compositions. How-

ever, we consider this conclusion as tentative. A more complete assessment of metal-saturation in natural magmatic systems will require a better understanding of the effects of factors like melt composition, *T*, and fS_2 on metal solubility in molten silicate.

Acknowledgements

We are grateful to Kevin Righter, Wim van Westrenen and an anonymous reviewer for their comments on the manuscript. Funding for this research was provided by grants to JMB from the Natural Sciences and Engineering Research Council of Canada and to WFM from the U.S. National Science Foundation and NASA.

References

[1] G.E. Brugmann, N.T. Arndt, A.W. Hofmann, H.J. Tobschall, Noble metal abundances in komatiite suites from Alexo, Ontario, and Gorgona Island, Colombia, Geochim. Cosmochim. Acta 51 (1987) 2159–2169.

[2] I.S. Puchtel, M. Humayun, Platinum group elements in Kostomuksha komatiites and basalts: implications for oceanic crust recycling and core–mantle interaction, Geochim. Cosmochim. Acta 64 (2000) 4227–4242.

[3] I.S. Puchtel, M. Humayun, Platinum group element fractionation in a komatiitic basalt lava lake, Geochim. Cosmochim. Acta 65 (2001) 2979–2994.

[4] I.S. Puchtel, M. Humayun, A.J. Campbell, R. Sproule, R.C.M. Lesher, Platinum group element geochemistry of komatiites from the Alexo and Pyke Hill areas, Ontario, Canada, Geochim. Cosmochim. Acta 68 (2004) 1361–1383.

[5] J.H. Crockett, Geochemistry of the platinum-group elements, Can. Inst. Min. Metall. Spec. Issue 23 (1981) 47–64.

[6] R.R. Keays, Palladium and iridium in komatiites and associated rocks, application to petrogenetic problems, in: N.T. Arndt, E.G. Nisbet (Eds.), Komatiites, Allen, London, 1982, pp. 435–458.

[7] I.O. Oshin, J.H. Crocket, Noble metals in Thetford Mines ophiolites, Quebec: Part 1. Distribution of gold, iridium, platinum, and palladium in the ultramafic and gabbroic rocks, Econ. Geol. 77 (1982) 1556–1570.

[8] S.J. Barnes, A.J. Naldrett, M.P. Gorton, The origin of the fractionation of the platinum group elements in terrestrial magmas, Chem. Geol. 53 (1985) 303–323.

[9] S.J. Barnes, C.P. Picard, The behaviour of platinum-group elements during partial melting, crystal fractionation, and sulphide segregation: an example from the Cape Smith Fold Belt, northern Quebec, Geochim. Cosmochim. Acta 57 (1993) 79–87.

[10] S.R. Hart, G.E. Ravizza, Os partitioning between phases in lherzolite and basalt, Earth Processes: Reading the Isotopic Code, AGU Monograph, vol. 95, 1996, pp. 123–133.

[11] W.D. Maier, S.-J. Barnes, Platinum-group elements in silicate rocks of the lower, critical and main zones at union section, Western Bushveld Complex, J. Petrol. 40 (1999) 1647–1671.

[12] J.M. Brenan, W.F. McDonough, C. Dalpe, Experimental constraints on the partitioning of rhenium and some platinum-group elements between olivine and silicate melt, Earth Planet. Sci. Lett. 212 (2003) 135–150.

[13] K. Righter, A.J. Campbell, M. Humayun, M.R.L. Hervig, Partitioning of Ru, Rh, Pd, Re, Ir and Au between Cr-bearing spinel, olivine, pyroxene and silicate melts, Geochim. Cosmochim. Acta 68 (2004) 867–880.

[14] R.J. Walker, S.B. Shirey, O. Stecher, Comparative Re–Os, Sm–Nd and Rb–Sr isotope and trace element systematics for Archean komatiite flow from Munro Township, Abitibi Belt, Ontario, Earth Planet. Sci. Lett. 87 (1988) 1–12.

[15] R.J. Walker, L.M. Echeverria, S.B. Shirey, M.F. Horan, Re–Os isotopic constraints on the origin of volcanic rocks, Gorgona Island, Colombia: Os isotopic evidence for ancient heterogeneities in the mantle, Contrib. Mineral. Petrol. 107 (1991) 150–162.

[16] R.J. Walker, M. Storey, A.C. Kerr, J. Tarney, N.T. Arndt, Implication of 187Os isotopic heterogeneities in a mantle plume: evidence from Gorgona island and Curaçao, Geochim. Cosmochim. Acta 63 (1999) 713–728.

[17] K.W. Burton, A. Gannoun, J.-L. Birk, C.J. Allegre, P. Schiano, R. Clocchiatti, O. Alard, The compatibility of rhenium and osmium in natural olivine and their behaviour during mantle melting and basalt petrogenesis, Earth Planet. Sci. Lett. 198 (2002) 63–76.

[18] R.H. Mitchell, R.R. Keays, Abundance and distribution of gold, palladium and iridium in some spinel and garnet lherzolites: implication for the nature and origin of precious metal-rich intergranular components in the upper mantle, Geochim. Cosmochim. Acta 45 (1981) 2425–2442.

[19] J.P. Lorand, R.R. Keays, J.L. Bodinier, Copper and noble metal enrichments across the lithosphere–asthenosphere boundary of mantle diapirs: evidence from the Lanzo lherzolite massif, J. Petrol. 34 (1993) 1111–1140.

[20] D.G. Pearson, S.B. Shirey, R.W. Carlson, F.R. Boyd, N.P. Pokhilenko, N. Shimizu, Re–Os, Sm–Nd, and Rb–Sr isotope evidence for thick Archean lithospheric mantle beneath the Siberian craton modified by multistage metasomatism, Geochim. Cosmochim. Acta 59 (1995) 959–977.

[21] A. Borisov, H. Palme, Experimental determination of the solubility of platinum in silicate melts, Geochim. Cosmochim. Acta 61 (1997) 4349–4357.

[22] A. Borisov, H. Palme, Solubility of noble metals in iron-containing silicate melts as derived from experiments on iron-free systems, Am. Min. 85 (2000) 1665–1673.

[23] A. Borisov, R.J. Walker, Os solubility in silicate melts: new efforts and results., Am. Min. 85 (2000) 912–917.

[24] T.B. Massalski, Binary Alloy Phase Diagrams, 2nd ed., ASM International, Materials Park, Ohio, 1990.

[25] W. Ertel, H.St.C. O'Neill, P.J. Sylvester, D.B. Dingwell, Solubilities of Pt and Rh in haplobasaltic silicate melt at 1300 °C, Geochim. Cosmochim. Acta 63 (1999) 2439–2449.
[26] W. Ertel, H.St.C. O'Neill, P.J. Sylvester, D.B. Dingwell, B. Spettel, The solubility of rhenium in silicate melts: implications for the geochemical properties of rhenium at high temperatures, Geochim. Cosmochim. Acta 65 (2001) 2161–2170.
[27] H.St.C. O'Neill, D. Dingwell, A. Borisov, B. Spettel, H. Palme, Experimental petrochemistry of some highly siderophile elements at high temperatures, and some implications for core formation and the mantle's early history, Chem. Geol. 120 (1995) 255–273.
[28] D.J. Lindstrom, J.H. Jones, Neutron activation analysis of multiple 10–100 μg glass samples from siderophile element partitioning experiments, Geochim. Cosmochim. Acta 60 (1996) 1195–1203.
[29] S.M. Eggins, L.P.J. Kinsley, J.M.M. Shelley, Deposition and element fractionation processes during atmospheric pressure laser sampling for analysis by ICPMS, Appl. Surf. Sci. 127–129 (1998) 278–286.
[30] A. Kilinic, I.S.E. Carmichael, M.L. Rivers, R.O. Sack, The ferric/ferrous ratio of natural silicate liquids equilibrated in air, Contrib. Mineral. Petrol. 83 (1983) 136–140.
[31] P.L. Roeder, R.F. Emslie, Olivine–liquid equilibrium, Contrib. Mineral. Petrol. 29 (1970) 275–289.
[32] A.J.G. Jurewicz, E.B. Watson, Cations in olivine: Part 1. Calcium partitioning and calcium–magnesium distribution between olivines and coexisting melts, with petrological applications, Contrib. Mineral. Petrol. 99 (1988) 176–185.
[33] J. Amosse, M. Allibert, W. Fischer, M. Piboule, Experimental study of the solubility of platinum and iridium in basic silicate melts — implications for the differentiation of platinum group elements during magmatic processes, Chem. Geol. 81 (1990) 45–53.
[34] A. Borisov, H. Palme, Solubility of iridium in silicate melts: new data from experiments with $Ir_{10}Pt_{90}$ alloys, Geochim. Cosmochim. Acta 59 (1995) 481–485.
[35] J. Amosse, M. Allibert, Partitioning of iridium and platinum between metals and silicate melts: evidence for passivation of the metals depending on fO_2, Geochim. Cosmochim. Acta 57 (1993) 2395–2398.
[36] A. Borisov, H. Palme, B. Spettel, Solubility of palladium in silicate melts: implications for core formation in the Earth, Geochim. Cosmochim. Acta 58 (1994) 705–716.
[37] A. Borisov, K. Nachtweyh, Ru solubility in silicate melts: experimental results in oxidizing region, Lunar Planet. Sci. XXIX (1998) (Abstract No. 1320).
[38] A. Borisov, H. Palme, Experimental determination of the solubility of Au in silicate melt, Mineral. Petrol. 56 (1996) 297–312.
[39] F. Farges, D.R. Neuville, G.E. Brown, Structural investigation of platinum solubility in silicate glasses, Am. Min. 84 (1999) 1562–1568.
[40] A. Borisov, Y. Lahaye, H. Palme, The effect of TiO_2 on Pd, Ni and Fe solubilities in silicate melts, Am. Min. 89 (2004) 564–571.
[41] P. Beattie, Systematics and energetics of trace-element partitioning between olivine and silicate melts: implications for the nature of mineral/melt partitioning, Chem. Geol. 117 (1994) 57–71.
[42] J. Blundy, B.J. Wood, Prediction of crystal–melt partition coefficients from elastic moduli, Nature 372 (1994) 452–454.
[43] J.A. Purton, J.D. Blundy, N.L. Allan, Computer simulation of high-temperature, forsterite–melt partitioning, Am. Min. 85 (2000) 1087–1091.
[44] L. Pauling, The Nature of the Chemical Bond, Cornell University Press, Ithaca, 1960.
[45] R.D. Shannon, C.T. Prewitt, Effective ionic radii in oxides and fluorides, Acta Cryst., B 25 (1969) 925–946.
[46] R.D. Shannon, C.T. Prewitt, Revised values of effective ionic radii, Acta Cryst., B 26 (1970) 1046–1048.
[47] B.J. Wood, J.D. Blundy, The effect of cation charge on crystal–melt partitioning of trace elements, Earth Planet. Sci. Lett. 188 (2001) 59–71.
[48] J.M. Brenan, E. Neroda, C.C. Lundstrom, H.F. Shaw, F.J. Ryerson, D.L. Phinney, Behaviour of boron, beryllium and lithium during melting and crystallization: constraints from mineral–melt partitioning experiments, Geochim. Cosmochim. Acta 62 (1998) 2129–2141.
[49] D.C. Harris, L.J. Cabri, The nomenclature of natural alloys of osmium, iridium and ruthenium based on new compositional data of alloys from world wide occurrences, Can. Mineral. 12 (1973) 104–112.
[50] H.M. Prichard, C.R. Neary, P.J. Potts, Platinum group minerals in the Shetland ophiolite, Metallogeny of Basic and Ultra Basic Rocks, Inst. of Mining Metall., London, UK, 1986, pp. 395–414.
[51] J. Torres-Ruiz, G. Garuti, M. Gazzotti, F. Gervilla, P. Fenoll Hach-Ali, Platinum-group minerals in chromitites from the Ojen lherzolite massif (Serrania de Ronda Beltic Cordillera, Southern Spain), Mineral. Petrol. 56 (1996) 25–50.
[52] S.J. Edwards, Harzburgites and refractory melts in the Lewis Hills massif, Bay of Islands ophiolite complex: the base-metals and precious-metals story, Can. Mineral. 28 (1990) 537–552.
[53] O. Legendre, T. Auge, Mineralogy of platinum-group mineral inclusions in chromitites from different ophiolite complexes, in: M.J. Gallagher, R.A. Ixer, C.R. Neary, H.M. Richards (Eds.), Metallogeny of Basic and Ultrabasic Rocks, Inst. Mining Metallurgy, London, U.K, 1986, pp. 361–375.
[54] G. von Gruenewaldt, L.J. Hulbert, A.J. Naldrett, Contrasting platinum-group element concentration patterns in cumulates of the Bushveld Complex, Miner. Depos. 24 (1989) 219–229.
[55] W.D. Maier, H.M. Prichard, S.-J. Barnes, P.C. Fisher, Compositional variation of laurite at Union Section in the Western Bushveld Complex, S. Afr. J. Geol. 102 (1999) 286–292.
[56] R.W. Talkington, B.R. Lipin, Platinum-group minerals in chromite seams of the Stillwater Complex, Montana, Econ. Geol. 81 (1986) 1179–1186.
[57] D.C. Peck, R.R. Keays, R.J. Ford, Direct crystallization of refractory platinum-group element alloys from boninitic magmas: evidence from western Tasmania, Aust. J. Earth Sci. 39 (1992) 373–387.

[58] J. Mungall, Coprecipitation of platinum-group minerals with chromite from silicate melts, 9th Annual Pt. Symposium, Billings, Montana, 2002.
[59] C.S. Finnigan, J.M. Brenan, Experimental evidence for the formation of PGE alloy inclusions in chromite by local reduction, GAC/MAC Annual Meeting, St. Catherine's, 2004, p. 72.
[60] D. Canil, Vanadium partitioning and the oxidation state of Archaean komatiite magmas, Nature 389 (1997) 842–845.
[61] D. Canil, H.St.C. O'Neill, D.G. Pearson, R.L. Rudnick, W.F. McDonough, D.A. Carswell, Ferric Fe in peridotites and mantle oxidation states, Earth Planet. Sci. Lett. 123 (1994) 205–220.
[62] J. Amosse, P. Dable, M. Allibert, Thermochemical behaviour of Pt, Ir, Rh and Ru vs. fO_2 and fS_2 in a basaltic melt. Implications for the differentiation and precipitation of these elements, Min. Pet. 68 (2000) 29–62.